Modulation of Magnetorheological Fluid Flow in Soft Robots Using Electropermanent Magnets

Kevin J. McDonald[1], Lorenzo Kinnicutt[1], Anna Maria Moran[2], and Tommaso Ranzani[1,3]

***Abstract*—Magnetorheological (MR) fluids, which stiffen in the presence of magnetic fields, have been shown to be an effective means for controlling the inflation of soft actuators. However, past efforts have largely focused on binary control. Proportional control schemes have faltered due to the difficulty in producing sufficient magnetic fields without requiring large amounts of electrical power. Electropermanent magnets (EPMs) offer one solution to this issue, since they can produce magnetic fields which are similar in magnitude to permanent magnets, they can be controlled electrically, but they do not require any power to hold their state. In this paper, we use EPMs to control the material properties of an MR fluid, allowing us to modulate the pressure within soft actuators. We demonstrate and quantify this behavior for several classes of soft actuators via bending and blocked force testing. We then demonstrate the ability to independently control the actuation of multiple-DoFs systems operating in both a binary and fully-modulated manner, thus providing an important step towards the development of reprogrammable, autonomous soft robots.**

***Index Terms*—Soft Robot Materials and Design; Hydraulic/Pneumatic Actuators**

I. Introduction

FLUIDICALLY actuated soft robots are widely used due to their compliance, dexterity, and high force output [1]. The cooperation of many degrees of freedom (DoFs) actuated in this manner allows for robots that are well suited to a variety of applications including minimally invasive surgery and navigation of complex terrains [2]–[5]. Multi-DoF fluidically actuated soft robots are typically controlled using an external pressure controller which is connected to the robot via a bundle of tubes, one for each actuator [4]–[6]. This introduces significant weight and volume while negatively impacting the dynamics of the robot and thus limiting its autonomy by requiring modulation of the robot's behavior to be done at the pressure source rather than at the point of actuation [7]. Therefore it is necessary to pursue control methods which preserve as much of a robot's intrinsic compliance as possible while allowing for real-time reprogrammability of complex behaviors, allowing a single robot to vary its behavior depending on the state of its controller.

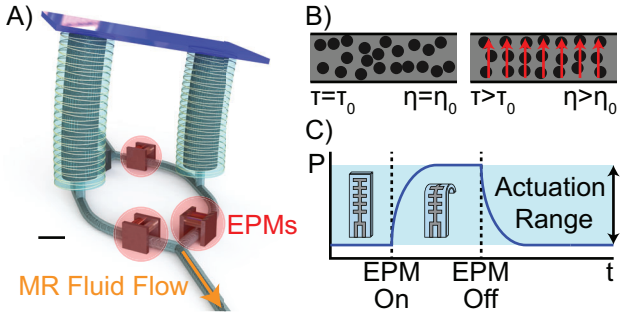

Figure 1. A) Rendering of a two-DoF, fully-modulated soft robotic platform controlled using an MR fluid and EPMs. The scale bar represents 1 cm. B) The particle-level behavior of the MR fluid in response to a magnetic field, indicating how the yield stress τ and viscosity η increase. C) The pressure response of a flowing MR fluid when a magnetic field is applied.

Recently, there has been an increased focus on introducing control hardware onboard the robots themselves by positioning valves closer to the point of actuation [8]. This can be done using commercially available rigid valves which perform at high pressures and operating frequencies at the expense of introducing hard materials which can act as points of failure due to the difference in stiffness compared to the soft robot itself [9]–[12]. Onboard valves have also used pressure driven techniques from microfluidics [13]–[17]. Other researchers have exploited viscous effects to control a robot's response to specific pressure wave inputs [18]–[20]. Similarly, smart fluids have been used to create valves which can modify the pressure in a soft actuator in response to an electrical control signal [21]–[27].

One such class of smart fluids are magnetorheological (MR) fluids [28], which have larger yield stresses than similar materials like electrorheological fluids [29]. MR fluids, mixtures of iron particles, a carrier fluid, and stabilizing additives, experience an increase in yield stress in the presence of a magnetic field. Modulating the strength of the magnetic field can be used to control the fluid's yield stress and in turn the pressure of the fluid flow. In a previous work, we exploited this behavior to inflate soft actuators connected to the flow channel [26]. This was achieved by manually placing permanent magnets in predetermined locations until motion of the actuators was achieved. However this approach was limited by the need to manually move the magnets, the inability to electronically control the pressure inside the

Manuscript received: September 9, 2021; Revised December 10, 2021; Accepted January 23, 2022.

This paper was recommended for publication by Editor Kyu-Jin Cho upon evaluation of the Associate Editor and Reviewers' comments. This work was partially supported by the National Science Foundation Research Experiences for Undergraduates Site in Integrated Nanomanufacturing, EEC-1852255

[1]K. J. McDonald, L. Kinnicutt, and T. Ranzani are with the Department of Mechanical Engineering, Boston University, Boston, MA 02215, USA

[2]A. M. Moran is with the Department of Physics, Mount Holyoke College, South Hadley, MA 01075, USA.

[3]T. Ranzani is with the Department of Biomedical Engineering and Materials Science and Engineering Division, Boston University, Boston, MA 02215, USA tranzani@bu.edu

Digital Object Identifier (DOI): see top of this page.

actuator, and the binary on/off nature of the fields applied. As such, it is necessary to explore alternate means of magnetic field generation that allow for hands-off operation and full modulation of an MR fluid controlled soft robot, enabling the pressure in multiple actuators to be controlled at the point of actuation. Electromagnets have been used in high-frequency, rigid MR valves [30], but they require large amounts of power to generate fields continuously while offering lower fields than their permanent counterparts [31].

Electropermanent magnets (EPMs) offer a promising solution. EPMs are an assembly of both permanent magnets and an electromagnet, providing the high fields and low power operation of a permanent magnet while allowing for an electrically controlled magnetic field like an electromagnet. EPMs have previously been used to create valves for pneumatic soft robots [32], [33]. EPMs have been used to create valves in MR fluid powered soft robots, but only binary on/off valves without full modulation of the pressure via magnetic field were demonstrated [25]. However, the ability to control and reprogram the behavior of multiple DoFs in a proportional manner in real time provides significant advantages for autonomous soft robots [8].

In this paper, we introduce a technique for modulating the pressure in soft fluidic actuators using MR fluids and EPMs (Fig. 1). By controlling the magnetic field exerted on a continuously flowing MR fluid we are able to tune its material properties and thus the flow pressure and the deformation of an attached soft actuator. EPMs allow us to precisely control the magnetic field electronically, allowing for reprogrammable, fully-modulated, proportional control of actuators' behavior at the point of actuation. This improves upon our previous efforts which relied on manually positioned permanent magnets and goes beyond the binary control demonstrated in the state-of-the-art [25], [26]. Proportionality allows us to control each DoF without adjusting the flow supplied by a pump. We demonstrate this technique on three classes of soft actuators and on multi-actuator architectures.

II. Design and Manufacturing

Any fluid which flows through a pipe will experience a pressure drop, ΔP, due to frictional losses. This ΔP increases with flow rate, but is largely due to the material properties of the fluid since more viscous materials exhibit larger ΔP for a given flow rate and pipe geometry. Recent research has exploited the ΔP associated with pipe geometries to control the bending of soft actuators [19]. The ΔP and flow rate also affect the dynamical response of a soft robot system [7]. However, the geometry and materials of the actuators themselves have perhaps an even larger effect on the overall performance [34].

Herein, we actively control the ΔP of a fluid flow via modulation of an MR fluid's material properties using magnetic fields (Fig. 1 B). High flow rates can allow for faster actuation, but the associated ΔP due to viscous effects can cause actuation without any magnetic field activation (Fig. 1 C).

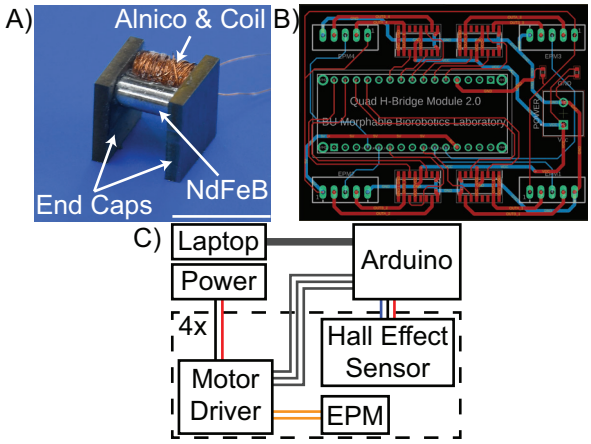

Figure 2. A) EPM, the scale bar represents 1 cm. B) The board layout of the custom four-EPM control circuit. The pinout for the Arduino is at center, with the power connection to the right, the motor drivers in the top and bottom and the headers for the EPMs and hall effect sensors in the corners. C) A schematic representation of the control circuit.

A. Electropermanent Magnets

EPMs are a combination of two permanent magnets, typically one neodymium and one alnico, and an electromagnet, all placed between two steel end caps [35] (Fig. 2 A). While the two permanent magnets have a nearly identical remanence (or residual magnetism), the neodymium magnet has a larger coercivity (i.e. resistance to change in magnetization) than the alnico magnet. A brief pulse from the electromagnet is then used to reorient the magnetic field of the alnico magnet. Depending on the orientation of the alnico magnet's field, the EPM can exert fields between its end caps which range from $0\,\mathrm{mT}$ to a maximum value determined by the constituent magnets' strengths and the geometry of the device. The alnico magnet component was manufactured using a $6.4\,\mathrm{mm}$ long Alnico 5 rod magnet with a diameter of $3.2\,\mathrm{mm}$ (McMaster, USA). The neodymium magnet was a Grade N42 axially magnetized neodymium disc magnet with a diameter of $3.2\,\mathrm{mm}$ and a length of $6.4\,\mathrm{mm}$ (K&J Magnetics, USA). The dimensions allowed for the soft robot tubing to pass between the end caps at the point of maximum field strength, yielding fields on the MR fluid comparable to the $\approx 40\,\mathrm{mT}$ exerted by the permanent magnets on the fluidic channels in [26]. The end caps ($15.9\,\mathrm{mm} \times 15.9\,\mathrm{mm} \times 1.6\,\mathrm{mm}$) were machined from grade A36 low-carbon steel (McMaster, USA). A 75-turn coil was wrapped around the alnico magnet using 36 gauge polyamide coated copper motor winding wire. The magnets were then adhered to the end caps using cyanoacrylate glue (Gorilla Glue, Inc., USA). Using a precision LCR meter (Agilent, USA), a representative EPM was determined to have an inductance of $76\,\mu\mathrm{H}$ and a series resistance of $5.6\,\Omega$.

B. EPM Control Circuit

Controlling the magnetic field of an EPM requires a precisely timed pulse of a known current. Furthermore, one must be able to reverse the polarity of the current to provide both magnetization and demagnetization of the alnico magnet. This can be achieved with a motor driver and microcontroller.

Two low current conductors connect the microcontroller to the motor driver to control the state and direction of the current to the electromagnet, which is provided via a separate, high-current supply. A separate motor driver is necessary for each EPM to be controlled independently. To characterize the EPMs, we used a commercially available motor driver (Handson Technology BTS7960) connected to an Arduino Uno and a benchtop power supply (B&K Precision 1671A) set to deliver 20 V. To control multiple EPMs, we manufactured a custom control board consisting of four motor driver chips (VNH7070BASTR, STMicroelectronics) and an Arduino Nano capable of full modulation of up to four EPMs (Fig. 2 B, C). The control board also provided connections for Hall effect sensors (DRV5055A3ELPGMQ1, Texas Instruments) to monitor the magnetic field strength at each EPM. The Arduino serial monitor was used to send control commands indicating an EPM identification number and the direction and duration of the current pulse.

C. Magnetorheological Fluid

The MR fluid was made using a solution of 0.2% by weight xanthan gum (Sigma Aldrich, G1253) in deionized water. This was mixed with 23% by volume of carbonyl iron particles (3 µm to 5 µm size, Skyspring Nanomaterials, 0990JH) and vortexed until homogenous. The xanthan gum served as a thixotropic agent to increase stability and reduce sedimentation of the iron particles.

D. Soft Actuators

Three classes of soft actuators were manufactured to evaluate the compatibility of the proposed fully-modulated control strategy with common soft actuator designs that have been evaluated and modeled in the literature [36], [37]. Planar soft actuators were manufactured layerwise out of silicone rubber using acrylic molds cut with a laser cutter. Each layer was 1.6 mm in thickness. Each actuator consisted of a layer of Ecoflex 00-30 and a strain limiting layer of Dragon Skin 20. Each silicone was mixed using a centrifugal mixer (ARE-310, Thinky, USA), poured into its respective mold, and cured in a 70 °C oven for 30 min. The two layers were bonded together by spin coating a 300 µm layer of Ecoflex 00-30 onto the strain limiting layer and curing it at 70 °C for 15 min. Silicone tubing with an inner diameter of 1.6 mm was inserted into the actuator's inlet and outlet and then sealed using Silpoxy (Smooth-On, USA). Fiber-reinforced soft actuators and PneuNets actuators were manufactured using Ecoflex 00-30 following the methods available from the Soft Robotics Toolkit [38].

III. Modeling

A full understanding of the behavior of MR fluids and their use in soft robots requires knowledge of the generation of the magnetic field, the field's effect on the fluid, and the resulting change in the flow behavior leading to an increase in pressure. Previous works have explored the effect of magnetic field on the fluid properties [26], [39], [40]. Here we provide simulations predicting the magnetic field produced by an EPM and a simplified means of understanding the effect a magnetized MR fluid has on flow behavior, allowing for comparison with established methods for exploiting viscous effects on pressure drops in soft robots.

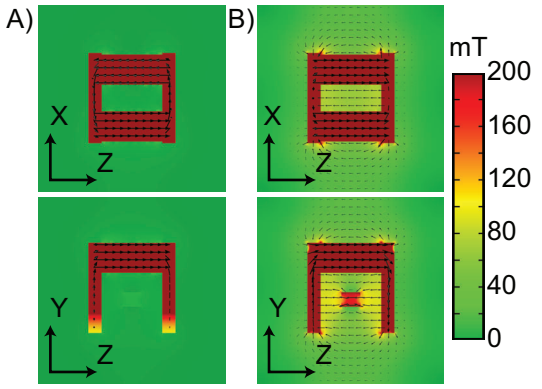

Figure 3. COMSOL simulation of an EPM with an MR fluid channel. A) EPM in its "off" state. B) EPM in its "on" state.

A. EPM Simulations

An EPM assembly with the same dimensions and magnetic properties as the physical magnet (per the manufacturers' specifications [41], [42]) was modeled using the Magnetic Fields, No Current physics module in COMSOL [43]. The Alnico magnet was assigned an anisotropic remanent flux density of 1.23 T in the Z-direction. This value was positive for the simulation of the EPM in its "on" state and negative for the simulation of the EPM in its "off" state. Intermediate states were not tested due to the nonlinear magnetic properties of the EPM. The neodymium magnet was assigned an anisotropic remanent flux density of 1.32 T in the positive Z-direction. A low-permeability gap of 500 µm was placed at the contact point between the magnets and end caps to simulate the glue thickness. For both the EPM in its "on" and "off" states, two simulations were run. The first had only empty space between the two end caps, but the second included a 2 mm × 1.5 mm channel of simulated MR fluid with a relative permeability of 10 (based on [25]) passing through the center. In all cases, a line was taken between the center of the two end caps, and the mean magnetic field was calculated. Simulation results are reported in Fig. 3. Without the channel of simulated MR fluid, the EPM produced a mean magnetic field of 2.7 mT in its "off" state and 77.4 mT in its "on" state. With the channel of simulated MR fluid, the EPM produced a mean magnetic field of 4.2 mT in its "off" state and 118.7 mT in its "on" state.

B. Effective Radius as a Model for MR Fluid Flow Behavior

MR fluids are commonly modeled as Bingham plastics, meaning that they do not flow until shear stresses surpass the material's yield stress, τ_0, after which the material flows like a fluid with viscosity η_0 with a "plug" profile. This flow behavior is modeled using the Buckingham-Reiner equation [44].

$$Q = \frac{\pi \Delta P R^4}{8\eta_0 L}\left[1 - \frac{4}{3}\left(\frac{2\tau_0 L}{\Delta P R}\right) + \frac{1}{3}\left(\frac{2\tau_0 L}{\Delta P R}\right)^4\right] \quad (1)$$

Where Q is the flow rate, ΔP is the change in pressure over length L, and R is the radius of the tube. For an MR fluid, τ_0 and η_0 are dependent on the strength of the magnetic field. In the absence of a magnetic field τ_0 of the MR fluid is negligible and $\eta_0 \approx 0.053\,\mathrm{Pa}\cdot\mathrm{s}$ [26]. For values of τ_0 equal to zero, Eq. 1 can be reduced to predict the expected radius for a given ΔP and η_0.

$$R = \left(\frac{8\eta_0 L Q}{\pi \Delta P}\right)^{1/4} \quad (2)$$

We can use Eq. 2 to calculate an effective radius for the MR fluid flow when a magnetic field is applied. An experiment was conducted where a $20\,\mathrm{mL\,min^{-1}}$ MR fluid flow was provided via a syringe pump through a $2.6\,\mathrm{mm}$ tube. An EPM was placed at the outflow of the tube, $6\,\mathrm{cm}$ from a pressure sensor. The magnetic field was modulated between $0\,\mathrm{mT}$ and $40\,\mathrm{mT}$ and the ΔP was recorded. Using Equation 2 an effective radius was calculated for each ΔP. These radii are the values that would cause the measured change in ΔP if the change were due only to a change in radius, not material properties. An effective occlusion, O_e was calculated as the ratio of the effective radius, R_e, to the actual tube radius, R_0 as $O_e = 100 \times \left(1 - \frac{R_e}{R_0}\right)$.

Fig. 4 A shows the pressure data collected experimentally and the derived values of effective occlusion. This metric is a simplification of the material behavior of the MR fluid as it models the ΔP due to the change in resistance in a MR fluid flowing in a channel due the magnetic field as a change in radius of the channel. This allows us to view the use of MR fluid to control soft robots much in the way as in [19], where tube lengths and radius were adjusted to influence the propagation of pressure through a robot. We can see that increasingly larger magnetic fields are necessary to decrease the effective radius to create larger pressure drops.

IV. EPM Characterization

To characterize the EPMs' performance, a test was conducted whereby the pulse length of the controlling current was varied while the magnetic field was recorded. The magnetic field between the EPM end caps was measured with a gaussmeter (Lake Shore Cryotronics Model 425). The pulse lengths supplied to the EPM were varied from $0\,\mu\mathrm{s}$ to $500\,\mu\mathrm{s}$, resulting in magnetic fields from $0\,\mathrm{mT}$ to the EPM's saturation point at $\approx 40\,\mathrm{mT}$. The exact saturation point varied slightly among each EPM due to minor differences in the manufacturing impacting their inductance, but each EPM exhibited a repeatable response to any given pulse length with a maximum standard deviation of $3.6\,\mathrm{mT}$ due primarily to the position of the probe during the test. The results from three trials are reported in Fig. 4 B.

This measured field was larger than the $25\,\mathrm{mT}$ field reported in [45], but lower than the value predicted via simulation. A second simulation was therefore run using the geometry of the EPM and MR fluid channel from [25], and the field matched their predicted value of approximately $225\,\mathrm{mT}$. Without any MR fluid, the predicted field dropped to $105.68\,\mathrm{mT}$. These simulations coupled with our direct measurements suggest that the simulated field overpredicts the actual field generated by an EPM due to irregularities and imperfections in the magnetic circuit inherent in the magnet assembly.

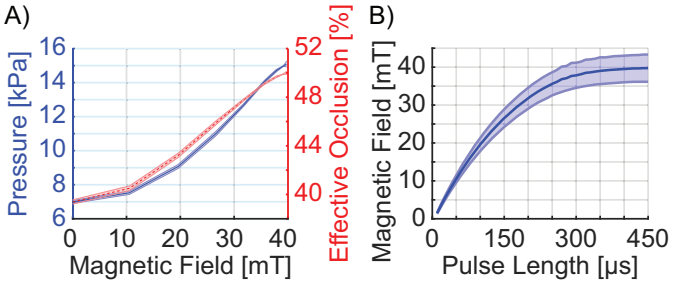

Figure 4. A) Experimental pressure and derived effective occlusion vs. magnetic field. B) Magnetic field vs. pulse length for an EPM, where mean and standard deviation represent a sample size of $N = 3$.

V. Actuator Characterization

The three soft bending actuator designs described in Section II-D were tested to determine their pressure and bending response while free to expand and force output during a blocked forced test. Each actuator was characterized across the full range of magnetic fields output by an EPM as determined in Section II-A. Doing so allows us to demonstrate that the EPM and MR fluid control method can be used to modulate the behavior of various soft actuator designs at the point of actuation without adjusting the parameters of the flow provided by the pump.

A. Actuator Bending and Pressure Characterization

For each actuator test, a continuous flow of MR fluid was provided by a syringe pump (Harvard Apparatus Pico Plus Elite) through a silicone rubber tube with a $1.59\,\mathrm{mm}$ inner diameter Fig. 5 A. The flow rate was chosen such that the flow pressure due to the fluid viscosity in the absence of an applied magnetic field would induce the actuator to be inflated to a point of neutral bending (as demonstrated by the actuation range represented schematically in Fig. 1 B). These pressures corresponded to a flow rate of $45\,\mathrm{mL\,min^{-1}}$ for the planar actuator, $25\,\mathrm{mL\,min^{-1}}$ for the fiber-reinforced actuator, and $20\,\mathrm{mL\,min^{-1}}$ for the PneuNets actuator. A pressure sensor (Nidec Copal Electronics P-7100-102GM5) was placed $10\,\mathrm{cm}$ from the syringe pump (Fig. 5 A). The actuators were placed $10\,\mathrm{cm}$ downstream of the pressure sensor using a T-junction, oriented such that they would bend horizontally, minimizing the effect of gravity. An EPM was placed $10\,\mathrm{cm}$ downstream of the soft actuator such that the tube was in between the two end caps. The tube emptied into an open reservoir $10\,\mathrm{cm}$ downstream of the EPM. Timing and control of the experiment was provided by a LabVIEW VI and National Instruments USB-6353 X-Daq, while the pulses to the EPM were controlled as described in Section II-B. The pump was

This article has been accepted for publication in a future issue of this journal, but has not been fully edited. Content may change prior to final publication. Citation information: DOI 10.1109/LRA.2022.3147873, IEEE Robotics and Automation Letters

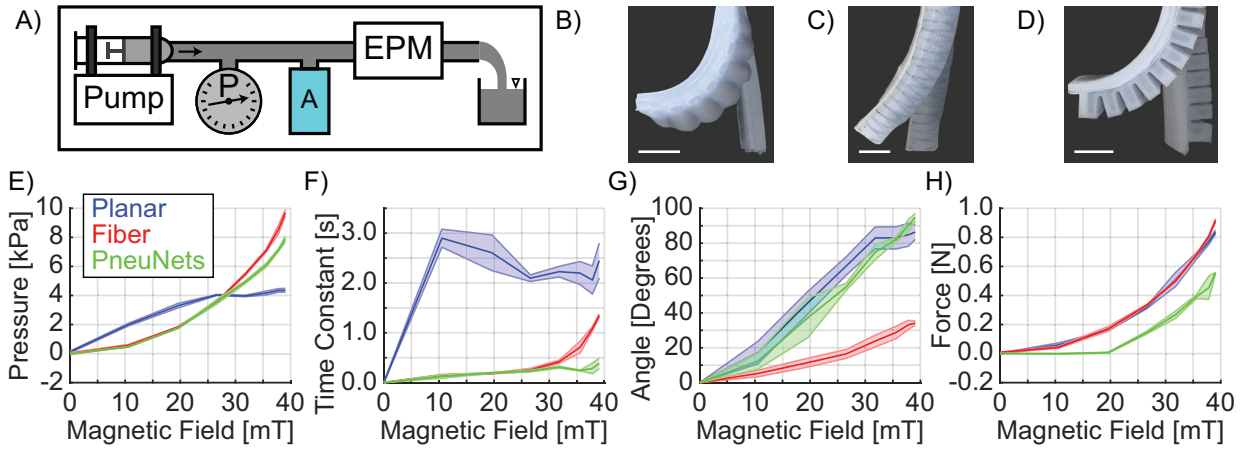

Figure 5. A) Schematic of the actuators test setup, B) the planar actuator, C) the fiber-reinforced actuator, and D) the PneuNets actuator. The images B)-D) show the "magnet on" states superimposed on the "magnet off" states. Scale bars represent 1 cm. E) Change in pressure vs. magnetic field, F) time constant vs. magnetic field, G) bending angle vs. magnetic field, and H) force vs. magnetic field. Means and standard deviations represent a sample size of $N = 3$.

first engaged for 10 s to allow the pressure in the flow to come to steady state with the EPM in its "off" state. Pressure data was then collected for 10 s with the EPM off. The control pulse was then sent to the EPM, which was set in its "on" state for 10 s. The EPM was then switched off and data collected for an additional 10 s while the actuator deflated, then the pump was disengaged. These timings were chosen based on the maximum volume of 60 mL that could be delivered via the syringe pump. At high magnetic fields, a longer period of time in the "magnet on" state would have allowed for higher maximum pressures. For each of the three actuators, the magnetization pulse lengths varied from 0 µs to 500 µs in increments of 50 µs, and the demagnetization pulse was always 500 µs of the opposite polarity to ensure complete demagnetization of the EPM. A delay of 100 µs was measured between the timing signal from the National Instruments DAQ and the EPM control pulse from the Arduino. Three trials were completed at each magnetization pulse length for each of the three actuators. Fig. 5 B–D shows the three types of actuators in the "magnet off" and "magnet on" states.

The pressure data for each experiment was compiled and analyzed in MATLAB. The average pressure over the last second before the magnetization pulse was sent determined the baseline pressure for every trial, representing the pressure in the "magnet off" regime. The average pressure over the last second before the demagnetization pulse was sent determined the maximum pressure for every trial, representing the pressure in the "magnet on" regime. The difference between these maximum and baseline pressures was used to determine the pressure change between the two regimes.

Fig. 5 E reports the actuator pressure for each of the three actuators plotted against magnetic field. The time constant for each trial was calculated as the time to reach 63.2% of the maximum pressure after the magnet was engaged to begin the "magnet on" regime. Fig. 5 F reports the time constant for each of the three actuators plotted against magnetic field. The time constant for the planar actuator was due to its larger internal volume change while inflating as a result of having fewer strain limiting features than the other two actuators. Means and standard deviations represent the results from three trials at each magnetization pulse length. This experiment verifies our ability to modulate the behavior of different standard actuator designs. The time constants compare favorably to the 250 s pressurization duration reported for the MR fluid valve in [25]. Our max pressure was lower due to the non-jamming nature of our proportional valve method, but it was in the same range as similar efforts to embed valves on soft robots [16], [19], [46]–[48]. The difference in pressure response between the different actuator types is in part due to their differing geometry and internal fluid volume, but is also due to the different flow rates necessary to induce neutral bending without an applied magnetic field.

Bending angle data was determined via analysis of still frames extracted from the experimental videos. Fig. 5 G reports the bending angle for each of the three actuators plotted against magnetic field.

B. Actuator Force Characterization

Blocked force experiments were run to evaluate the ability to electronically control and modulate the force output of each soft actuator design when pressurized using a continuously flowing MR fluid and an EPM. The test setup described in Section V-A was modified such that the soft actuators would bend in the vertical direction. A force sensor (ATI Nano 17) was mounted beneath the actuators. Pieces of acrylic provided a rigid surface above the actuators and a 1 cm × 2 cm plate for the tip of the actuators to act against, similar to [36].

A LabVIEW VI and National Instruments USB-6353 X-Daq were used control the experiment and provide precise timing for the activation of the Arduino's microsecond EPM control pulse. The timing remained identical, with a 10 s pre-pressurization, 10 s with the EPM in the "off" state, 10 s with the EPM in the "on" state, and 10 s of deflation time. The magnetization pulse lengths again varied from 0 µs to 500 µs in increments of 50 µs for each of the three actuators. Pressure

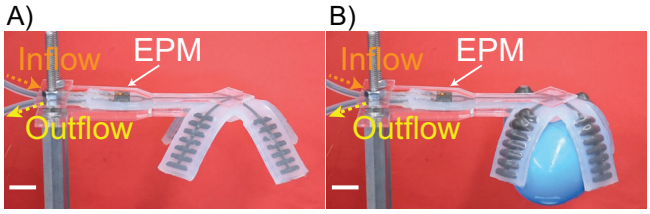

Figure 6. A soft gripper A) in the "magnet off" state and B) in the "magnet on" state, holding a 10 g egg. Scale bars represent 1 cm

and force data were collected throughout. Three trials were completed at each pulse length for each of the three actuators.

The average force over the last second before the magnetization pulse was sent determined the baseline force for every trial, representing the force in the "magnet off" regime. The average force over the last second before the demagnetization pulse was sent determined the maximum force for every trial, representing the force in the "magnet on" regime. The difference between these maximum and baseline forces was used to determine the force change between the two regimes. Fig. 5 H reports the blocked force for each of the three actuators plotted against magnetic field. The PneuNets actuator did not exert any force at low fields since it experienced very little expansion in the z-direction whereas the other two actuators experienced some expansion before bending. Means and standard deviations represent the results from three trials at each magnetization pulse length.

VI. Multi-DoF Control and Modulation

A. 1-DoF Coupled Actuation Gripper

A gripper was manufactured according to the method described in Section II-D. An EPM was built into the gripper such that its end caps were positioned on either side of the channel leading to the outlet tube and the MR fluid would flow between them. A syringe pump (Harvard Apparatus Pico Plus Elite) provided a continuous flow of MR fluid at a rate of $25\,\mathrm{mL\,min^{-1}}$. Fig. 6 A shows the gripper's "magnet off" state and Fig. 6 B shows a 10 g object grasped in the gripper's "magnet on" state. The gripper was not optimized for holding heavy or complex objects, and is meant only to serve as a demonstration of EPM-controlled coupled actuation.

B. Three Actuator Binary Control

The number of controllable DoFs can be maximized by using binary control in lieu of full modulation. Three fiber-reinforced soft actuators (A_1, A_2, and A_3 in Fig. 7) were manufactured using Ecoflex 00-50 (Smooth-On). These were connected together at a single node connected to a channel of continuously flowing MR fluid provided by a peristaltic pump (Fisherbrand GP1000). An EPM was placed around each of the tubes connected to the actuators (EPM_a, EPM_b, EPM_c), and an additional EPM, EPM_d, was placed downstream of the node to control the flow pressure (Fig. 7 A). Given sufficient drivers to control an arbitrary number of EPMs, n binary actuators connected to a single pressure node would require $n+1$ EPMs. The EPMs were controlled as described in

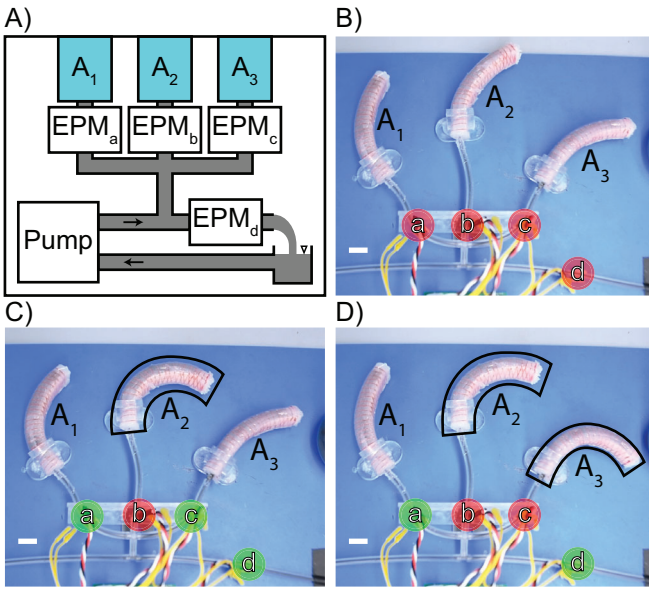

Figure 7. A) A schematic of the layout to control three binary DoFs (A_1, A_2, and A_3) with one EPM each (EPM_a, EPM_b, EPM_c) and one shared EPM, EPM_d. B) Unactuated state. C) A_2, and D) A_2 and A_3 are actuated. Red and green circles indicate EPMs in the "off" and "on" state respectively. Scale bars represent 1 cm

Section II-B, which allowed for four EPMs to be controlled simultaneously. By sending 500 µs pulses to the EPMs, the actuators could be engaged and disengaged in a binary manner, allowing for any combination of bending states. Since the EPMs function as normally-closed switches (i.e. the magnetic field must be turned on to block or obstruct the flow), the states of A_1, A_2, and A_3 are the opposite of the states of EPM_a, EPM_b, and EPM_c when the flow EPM, EPM_d, is engaged. If the flow EPM, EPM_d, is off, no actuators bend regardless of the states of EPM_a, EPM_b, and EPM_c. The flow provided by the peristaltic pump was constant when inflating the actuators. Fig. 8 A shows an electrical circuit analogous to this setup. Fig. 7 B-D shows a selection of the bending states achieved in this way.

C. Fully-Modulated Two Actuator Platform

Fully-modulated, independent control of multiple DoFs allows for real-time reprogramming of actuator behavior without adjusting flow parameters at the pump. In contrast to the binary control architecture in Section VI-B, controlling n fully-modulated actuators requires $2n$ EPMs. With the actuators connected in parallel, each requires one upstream EPM and one downstream EPM. The downstream EPM directly controls the pressure in the actuator, and the upstream EPM controls the resistance in the channel such that all channels have the same fluid resistance. This can be thought of as equivalent to an electrical circuit consisting of voltage dividers connected in parallel (Fig. 8 B). As the value of each electrical resistor can be adjusted to maintain an equal current in each branching path, so too can the EPMs be used to maintain an equal flow rate past each actuator. Two extending fiber-reinforced actuators, A_1 and A_2, were manufactured out of Ecoflex 00-

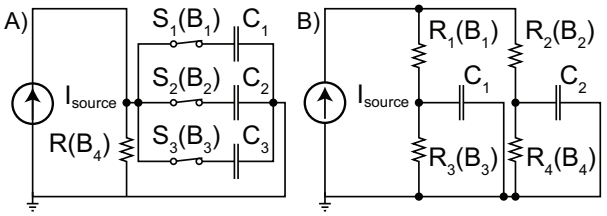

Figure 8. Electrical analogy of the fluidic systems in A) Section VI-B and B) Section VI-C. The current source, I_{source}, represents the fluid flow. The resistors, R, are analogous to the EPMs and capture the dependence of the flow resistance on the magnetic field. The normally-closed switches, S, are EPMs modulated in a binary manner. The capacitors, C, represent the soft actuators. The electrical ground models the open fluid reservoir.

20 (Smooth-On) using a custom 3D-printed mold. These were oriented vertically and used to support an acrylic plate. A peristaltic pump (Fisherbrand GP1000) was used to provide a continuous flow of MR fluid. The EPMs (EPM_a, EPM_b, EPM_c, EPM_d) were then used to modulate the pressure in the actuators, allowing the platform to change both its elevation and angle. Fig. 9 A shows a schematic of the EPM configuration and Fig. 9 B-G show selected states from this test. This experiment showed the ability to individually modulate the behavior of multiple DoFs without adjusting the parameters of the flow supplied at the pump. The angle and elevation of the platform were controlled directly via the modulation of the two actuators' pressure. This would not have been possible with binary control without adjusting the flow parameters at the pump.

VII. Conclusions

In this paper we demonstrated the use of a continuously flowing MR fluid and EPMs to embed fully-modulated, electronic control in multi-DoF soft robots. By controlling the magnetic field we were able to adjust the MR fluid's material properties, in turn controlling the pressurization of several classes of soft actuators. Standard actuator designs were evaluated for motion and force output and were found to have performance in terms of bending, force, and pressure on par with other onboard valve technologies [16], [19], [46]–[48]. However, our objective was not to maximize the efficiency of the actuators tested, and longer tests would have yielded higher values for stroke and force. These results support the specific goal of achieving fully-modulated control of soft actuators using MR fluids and EPMs. As with any soft robot control method, specific values of bending angle and force at a given pressure are dependent on an actuator's geometry and constituent materials. In all cases, magnetic fields were applied using EPMs, allowing for electrical control and modulation of the field strength. In this way multiple actuators could be controlled in either a binary or proportional manner. These multi-actuator systems included a gripper with four coupled DoFs and one EPM, an array of three binary-operation actuators with four EPMs, and a 2-DoF platform robot with four EPMs. Together these prove the ability to implement fully proportional fluidic control at the point of actuation in multi-actuator robotic systems via the modulation of material properties.

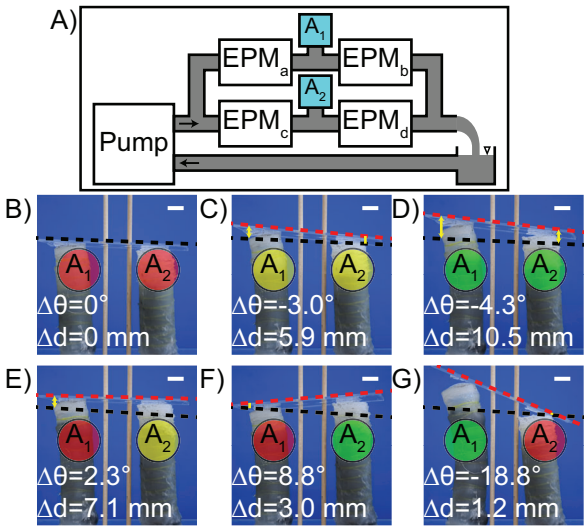

Figure 9. A) Schematic of the layout to control two proportional DoFs. B) A_1 and A_2 in their initial state, C) A_1 and A_2 partially inflated, D) A_1 and A_2 fully inflated, E) A_2 modulated to partial inflation with A_1 uninflated, F) A_2 fully inflated with A_1 uninflated, and G) A_1 fully inflated with A_2 uninflated. The red, yellow, and green circles represent actuators modulated to no, partial, and full inflation, respectively. The black and red dashed lines denotes initial and final position, respectively. Angle, θ, is taken from the red line as drawn. A_1 expanded more due to manufacturing inconsistencies. Scale bars represent $1\,\mathrm{cm}$.

The EPMs consumed no power except when switching their states, which only required $50\,\mathrm{mJ}$. While showing promise in allowing on-board fluidic control via full electronic modulation of pressure, presently MR fluids are not an ideal technique for the rapid actuation of soft robots. Fig. 5 F shows that the planar actuator had a time constant between $2\,\mathrm{s}$ and $3\,\mathrm{s}$, but the fiber-reinforced and PneuNets actuators had time constants below $1\,\mathrm{s}$. Optimization of response time is thus dependent on actuator design. However, our results are faster than [25], which shows inflation times over $200\,\mathrm{s}$ with a comparable technology. Higher flow rates allow for faster actuation, but they also have an inherently larger pressure drop due to viscous effects. One could manufacture actuators that inflate at these higher pressures, but only if it were also possible to control larger magnetic fields as well. The flow rate sets the floor of an actuator's operational pressure range, but the magnetic field sets the ceiling. Only by carefully balancing the flow parameters, actuator mechanics, and magnetic field can one design a system that has a robust response. Computational tools, such as discrete element modeling [25], [49], will be an important tool in solving this problem.

References

[1] P. Polygerinos, N. Correll, S. A. Morin, B. Mosadegh, C. D. Onal, K. Petersen, M. Cianchetti, M. T. Tolley, and R. F. Shepherd, "Soft robotics: Review of fluid-driven intrinsically soft devices; manufacturing, sensing, control, and applications in human-robot interaction," *Adv. Eng. Mater.*, vol. 19, no. 12, 2017.

[2] M. Cianchetti, T. Ranzani, G. Gerboni, T. Nanayakkara, K. Althoefer, P. Dasgupta, and A. Menciassi, "Soft robotics technologies to address shortcomings in today's minimally invasive surgery: The STIFF-FLOP approach," *Soft Robot.*, vol. 1, no. 2, pp. 122–131, 2014.

[3] C. Laschi, B. Mazzolai, and M. Cianchetti, "Soft robotics: Technologies and systems pushing the boundaries of robot abilities," *Sci. Robot.*, vol. 1, no. 1, pp. 1–12, 2016.

[4] R. F. Shepherd, F. Ilievski, W. Choi, S. A. Morin, A. A. Stokes, A. D. Mazzeo, X. Chen, M. Wang, and G. M. Whitesides, "Multigait soft robot," *Proc. Nat. Acad. Sci.*, vol. 108, no. 51, pp. 20 400–20 403, 2011.

[5] A. Yin, H. Ching Lin, J. Thelen, B. Mahner, T. Ranzani, H.-C. Lin, J. Thelen, B. Mahner, and T. Ranzani, "Combining locomotion and grasping functionalities in soft robots," *Adv. Intell. Sys.*, vol. 1, no. 8, pp. 1–7, 2019.

[6] A. A. Stokes, R. F. Shepherd, S. A. Morin, F. Ilievski, and G. M. Whitesides, "A hybrid combining hard and soft robots," *Soft Robot.*, vol. 1, no. 1, pp. 70–74, 2014.

[7] S. Joshi and J. Paik, "Pneumatic supply system parameter optimization for soft actuators," *Soft Robot.*, vol. 8, no. 2, pp. 152–163, 2021.

[8] K. McDonald and T. Ranzani, "Hardware methods for onboard control of fluidically actuated soft robots," *Frontiers in Robot. and AI*, vol. 8, pp. 1–19, 2021.

[9] M. T. Tolley, R. F. Shepherd, M. Karpelson, N. W. Bartlett, K. C. Galloway, M. Wehner, R. Nunes, G. M. Whitesides, and R. J. Wood, "An untethered jumping soft robot," in *IEEE Int. Conf. Intell. Robot. Sys.*, 2014, pp. 561–566.

[10] J. W. Booth, J. C. Case, E. L. White, D. S. Shah, and R. Kramer-Bottiglio, "An addressable pneumatic regulator for distributed control of soft robots," in *IEEE Int. Conf. Soft Robot.*, Livorno, Italy, 2018, pp. 25–30.

[11] G. Gerboni, T. Ranzani, A. Diodato, G. Ciuti, M. Cianchetti, and A. Menciassi, "Modular soft mechatronic manipulator for minimally invasive surgery (MIS): overall architecture and development of a fully integrated soft module," *Meccanica*, vol. 50, no. 11, pp. 2865–2878, 2015.

[12] A. D. Marchese, C. D. Onal, and D. Rus, "Autonomous soft robotic fish capable of escape maneuvers using fluidic elastomer actuators," *Soft Robot.*, vol. 1, no. 1, pp. 75–87, 2014.

[13] M. Wehner, R. L. Truby, D. J. Fitzgerald, B. Mosadegh, G. M. Whitesides, J. A. Lewis, and R. J. Wood, "An integrated design and fabrication strategy for entirely soft, autonomous robots," *Nature*, vol. 536, no. 7617, pp. 451–455, 2016.

[14] S. T. Mahon, A. Buchoux, M. E. Sayed, L. Teng, and A. A. Stokes, "Soft robots for extreme environments: Removing electronic control," in *IEEE Int. Conf. Soft Robot.*, 2019, pp. 782–787.

[15] N. W. Bartlett, K. P. Becker, and R. J. Wood, "A fluidic demultiplexer for controlling large arrays of soft actuators," *Soft Matter*, 2020.

[16] P. Rothemund, A. Ainla, L. Belding, D. J. Preston, S. Kurihara, Z. Suo, and G. M. Whitesides, "A soft, bistable valve for autonomous control of soft actuators," *Sci. Robot.*, vol. 3, no. 16, pp. 1–10, 2018.

[17] D. J. Preston, P. Rothemund, H. J. Jiang, M. P. Nemitz, J. Rawson, Z. Suo, and G. M. Whitesides, "Digital logic for soft devices," *Proc. Nat. Acad. Sci.*, vol. 116, no. 16, pp. 7750–7759, 2019.

[18] Y. Matia, T. Elimelech, and A. D. Gat, "Leveraging internal viscous flow to extend the capabilities of beam-shaped soft robotic actuators," *Soft Robot.*, vol. 4, no. 2, pp. 126–134, 2017.

[19] N. Vasios, A. J. Gross, S. Soifer, J. T. Overvelde, and K. Bertoldi, "Harnessing viscous flow to simplify the actuation of fluidic soft robots," *Soft Robot.*, 2019.

[20] A. Di Lallo, M. G. Catalano, M. Garabini, G. Grioli, M. Gabiccini, and A. Bicchi, "Dynamic morphological computation through damping design of soft continuum robots," *Frontiers in Robot. and AI*, vol. 6, no. April, pp. 1–19, 2019.

[21] A. Zatopa, S. Walker, and Y. Menguc, "Fully soft 3D-printed electroactive fluidic valve for soft hydraulic robots," *Soft Robot.*, vol. 5, no. 3, pp. 258–271, 2018.

[22] A. Sadeghi, L. Beccai, and B. Mazzolai, "Innovative soft robots based on electro-rheological fluids," *IEEE Int. Conf. Intell. Robot. Sys.*, pp. 4237–4242, 2012.

[23] N. Bira, Y. Menguc, and J. R. Davidson, "3D-printed electroactive hydraulic valves for use in soft robotic applications," *IEEE Int. Conf. Robot. Automat.*, pp. 11 200–11 206, 2020.

[24] A. Tonazzini, A. Sadeghi, and B. Mazzolai, "Electrorheological valves for flexible fluidic actuators," *Soft Robot.*, vol. 3, no. 1, pp. 34–41, 2016.

[25] T. Leps, P. E. Glick, D. Ruffatto III, A. Parness, M. T. Tolley, and C. Hartzell, "A low-power, jamming, magnetorheological valve using electropermanent magnets suitable for distributed control in soft robots," *Smart Mater. Struct.*, vol. 29, no. 10, pp. 1–13, 2020.

[26] K. McDonald, A. Rendos, S. Woodman, K. A. Brown, and T. Ranzani, "Magnetorheological fluid-based flow control for soft robots," *Adv. Intell. Sys.*, vol. 2, no. 11, pp. 1–8, 2020.

[27] R. Balak and Y. Mazumdar, "Bistable valves for MR fluid-based soft robotic actuation systems," *IEEE Robot. Autom. Lett.*, vol. 6, no. 4, pp. 8285–8292, 2021.

[28] S. Genc and pradeep Phule, "Rheological properties of magnetorheological fluids," *Smart Mater. Struct.*, vol. 140, no. 11, pp. 140–146, 2002.

[29] J. M. Ginder, L. Davis, and L. Elie, "Rheology of magnetorheological fluids: Models and measurements," *Int. J. Modern Phys. B*, vol. 10, no. 23 & 24, pp. 3293–3303, 1996.

[30] E. Kostamo, J. Kostamo, J. Kajaste, and M. Pietola, "Magnetorheological valve in servo applications," *J. Intell. Mater. Syst. Struct.*, vol. 23, no. 9, pp. 1001–1010, 2012.

[31] T. N. Do, H. Phan, T. Q. Nguyen, and Y. Visell, "Miniature soft electromagnetic actuators for robotic applications," *Adv. Functional Mater.*, vol. 28, no. 18, pp. 1–11, 2018.

[32] A. D. Marchese, C. D. Onal, and D. Rus, "Towards a self-contained soft robotic fish: On-board pressure generation and embedded electropermanent magnet valves," in *13th Int. Symp. Exp. Robot.*, 2013, pp. 41–54.

[33] ——, "Soft robot actuators using energy-efficient valves controlled by electropermanent magnets," in *IEEE Int. Conf. Intell. Robot. Sys.*, 2011, pp. 756–761.

[34] A. A. Stanley, A. Amini, C. Glick, N. Usevitch, and Y. M. J. Keller, "Lumped-parameter response time models for pneumatic circuit dynamics," *J. Dyn. Sys., Meas. Control*, vol. 143, no. 5, pp. 1–11, 2021.

[35] A. Knaian, "Electropermanent magnetic connectors and actuators: devices and their application in programmable matter," PhD Dissertation, Massachusetts Institute of Technology, 2010.

[36] P. Polygerinos, Z. Wang, J. T. Overvelde, K. C. Galloway, R. J. Wood, K. Bertoldi, and C. J. Walsh, "Modeling of soft fiber-reinforced bending actuators," *IEEE Trans. Robot.*, vol. 31, no. 3, pp. 778–789, 2015.

[37] Z. Liu, F. Wang, S. Liu, Y. Tian, and D. Zhang, "Modeling and analysis of soft pneumatic network bending actuators," *IEEE/ASME Trans. Mechatronics*, vol. 26, no. 4, pp. 2195–2203, 2021.

[38] Soft Robotics Toolkit, "Soft robotics toolkit." [Online]. Available: https://softroboticstoolkit.com/

[39] A. Rendos, S. Woodman, K. McDonald, T. Ranzani, and K. A. Brown, "Shear thickening prevents slip in magnetorheological fluids," *Smart Mater. Struct.*, vol. 29, no. 7, 2020.

[40] A. Rendos, R. Li, S. Woodman, X. Ling, and K. A. Brown, "Reinforcing magnetorheological fluids with highly anisotropic 2D materials," *ChemPhysChem*, pp. 1–7, 2020.

[41] McMaster-Carr, "Alnico disc magnet thickness magnetized, 4" thick, 1/8" OD, 0.3 lbs. maximum pull," 2021. [Online]. Available: https://www.mcmaster.com/5852K11/

[42] I. K&J Magnetics, "Neodymium magnet physical properties," 2021. [Online]. Available: https://www.kjmagnetics.com/specs.asp

[43] COMSOL, "The magnetic fields, no currents interface." [Online]. Available: https://doc.comsol.com/5.5/doc/com.comsol.help.acdc/acdc_ug_magnetic_fields.08.056.html

[44] R. B. Bird, G. C. Dai, and B. J. Yarusso, "The rheology and flow of viscoplastic materials," *Rev. Chem. Eng.*, vol. 1, no. 1, 1983.

[45] J. I. Padovani, S. S. Jeffrey, and R. T. Howe, "Electropermanent magnet actuation for droplet ferromicrofluidics," *Technol.*, vol. 04, no. 02, pp. 110–119, 2016.

[46] S. Song, S. Joshi, and J. Paik, "CMOS-inspired complementary fluidic circuits for soft robots," *Adv. Sci.*, vol. 2100924, pp. 1–14, 2021.

[47] S. Xu, Y. Chen, N.-s. P. Hyun, K. P. Becker, and R. J. Wood, "A dynamic electrically driven soft valve for control of soft hydraulic actuators," *Proc. Nat. Acad. Sci.*, vol. 118, no. 34, pp. 1–9, 2021.

[48] L. Jin, A. E. Forte, and K. Bertoldi, "Mechanical valves for on-board flow control of inflatable robots," *Adv. Sci.*, vol. 2101941, pp. 1–8, 2021.

[49] T. Leps and C. Hartzell, "High fidelity, discrete element method simulation of magnetorheological fluids using accurate particle size distributions in LIGGGHTS extended with mutual dipole method," *Mater. Res. Express*, vol. 8, no. 8, 2021.